© 2016. Published by The Company of Biologists Ltd | Journal of Cell Science (2016) 129, 2841-2851 doi:10.1242/jcs.186247

RESEARCH ARTICLE

CCN6 regulates mitochondrial function

Milan Patra[1], Sushil K. Mahata[2,3], Deepesh K. Padhan[1] and Malini Sen[1,*]

ABSTRACT

Despite established links of CCN6, or Wnt induced signaling protein-3 (WISP3), with progressive pseudo rheumatoid dysplasia, functional characterization of CCN6 remains incomplete. In light of the documented negative correlation between accumulation of reactive oxygen species (ROS) and CCN6 expression, we investigated whether CCN6 regulates ROS accumulation through its influence on mitochondrial function. We found that CCN6 localizes to mitochondria, and depletion of CCN6 in the chondrocyte cell line C-28/I2 by using siRNA results in altered mitochondrial electron transport and respiration. Enhanced electron transport chain (ETC) activity of CCN6-depleted cells was reflected by increased mitochondrial ROS levels in association with augmented mitochondrial ATP synthesis, mitochondrial membrane potential and Ca^{2+}. Additionally, CCN6-depleted cells display ROS-dependent PGC1α (also known as PPARGC1A) induction, which correlates with increased mitochondrial mass and volume density, together with altered mitochondrial morphology. Interestingly, transcription factor Nrf2 (also known as NFE2L2) repressed CCN6 expression. Taken together, our results suggest that CCN6 acts as a molecular brake, which is appropriately balanced by Nrf2, in regulating mitochondrial function.

KEY WORDS: CCN6, Mitochondria, PGC1α, Nrf2

INTRODUCTION

CCN6, or Wnt-induced signaling protein 3 (WISP3), is a 354-amino-acid protein that can function both intracellularly and extracellularly (Brigstock et al., 2003; Davis et al., 2006; Miller and Sen, 2007; Pal et al., 2012; Perbal, 2013; Repudi et al., 2013). WISP3 gets its name from its sequence homology with other WISP (CCN)-family members that are induced by Wnt1 (Pennica et al., 1998; Sen et al., 2004). CCN6 appears to be the preferred name for WISP3, as suggested and published by the International CCN Society (Brigstock et al., 2003). A signal peptide at the N-terminus of CCN6 is followed sequentially by the insulin growth factor binding protein (IGFBP) domain, the Von Willebrand factor type C (VWC) repeat domain, the thrombospondin type I (THSP1) repeat domain and the cysteine knot domain (Hurvitz et al., 1999; Pennica et al., 1998). Although the IGFBP domain of CCN6 indicates possible interactions with IGF, the presence of other domains alludes to the occurrence of intermolecular interactions of a diverse nature through disulfide bridging and oligomerization (Engel, 2004; Hurvitz et al., 1999).

[1]Cancer Biology and Inflammatory Disorder Division, CSIR-Indian institute of Chemical Biology, 4-Raja S.C. Mullick Road, Jadavpur, Kolkata 700032, India. [2]Metabolic Physiology and Ultrastructure Biology Laboratory, University of California, San Diego, CA 92093-0732, USA. [3]Veterans Affairs San Diego Healthcare System, San Diego, CA 92161, USA.

*Author for correspondence (msen@iicb.res.in; senmalini@yahoo.com)

M.P., 0000-0001-6870-9938; D.K.P., 0000-0003-2159-5800; M.S., 0000-0001-5903-5943

Received 16 January 2016; Accepted 8 April 2016

Mutations within the CCN6 coding sequence are linked to a skeletal disorder termed progressive pseudo rheumatoid dysplasia (PPRD), which is characterized by progressive cartilage loss and irregularities in bone growth (Dalal et al., 2012; Ekbote et al., 2013; Garcia Segarra et al., 2012; Hurvitz et al., 1999; Liu et al., 2015; Luo et al., 2015; Yang et al., 2013). The several mutations associated with PPRD, identified thus far, span across the different domains of CCN6, implying that all the domains of CCN6 contribute to its overall function. On account of the established link of CCN6 with PPRD, a comprehensive characterization of its function at the molecular level is important. CCN6 has been shown to modulate both IGF1-induced as well as basal expression of cartilage hypertrophy markers, such as reactive oxygen species (ROS) (Miller and Sen, 2007; Repudi et al., 2013). Other functions of CCN6 that might be useful in the context of cartilage growth and/or maintenance remain to be deciphered.

Given its influence on total cellular ROS accumulation (Miller and Sen, 2007; Repudi et al., 2013), we wanted to investigate if CCN6 controls mitochondrial ROS by regulating the mitochondrial electron transport chain (ETC). Perhaps the loss of a functional cartilage and the aberrant matrix mineralization associated with CCN6 mutations in individuals with PPRD (Dalal et al., 2012; Ekbote et al., 2013; Garcia Segarra et al., 2012; Hurvitz et al., 1999; Liu et al., 2015; Luo et al., 2015; Yang et al., 2013) are due to an imbalance in cell differentiation and/or hypertrophy, arising partly from altered mitochondrial function. Accordingly, it is essential to estimate the influence of wild-type CCN6 on the activity of mitochondrial electron transport. It is also crucial to understand how CCN6 expression synchronizes with its function. Therefore, in the current study, we explored if and how CCN6 influences mitochondrial function, and examined regulation of CCN6 expression.

RESULTS

CCN6 controls the steady-state levels of mitochondrial ROS, ATP and Ca^{2+}

In the light of previous findings demonstrating CCN6 as regulating total cellular ROS (Miller and Sen, 2007; Repudi et al., 2013), we examined if CCN6 influences mitochondrial ROS accumulation in association with mitochondrial ATP synthesis and Ca^{2+} at the steady state. Our investigation was furthermore prompted by several reports documenting the interrelation of mitochondrial ROS, ATP and Ca^{2+} (Brookes et al., 2004; Lehninger, 1970).

Upon depletion of CCN6 in the chondrocyte line C-28/I2 through transfection of small interfering (si)RNAs (CCN6 siRNA), a moderately amplified mitochondrial ROS response was detected by using MitoTracker CMH_2Xros, as compared to control upon flow cytometry analysis (Fig. 1A). Depletion of CCN6 expression in CCN6-siRNA-transfected C-28/I2 cells was demonstrated by performing both reverse-transcriptase (RT)-PCR and immunoblotting analysis on RNA and protein harvested from

Journal of Cell Science (2016) 129, 2841-2851 doi:10.1242/jcs.186247

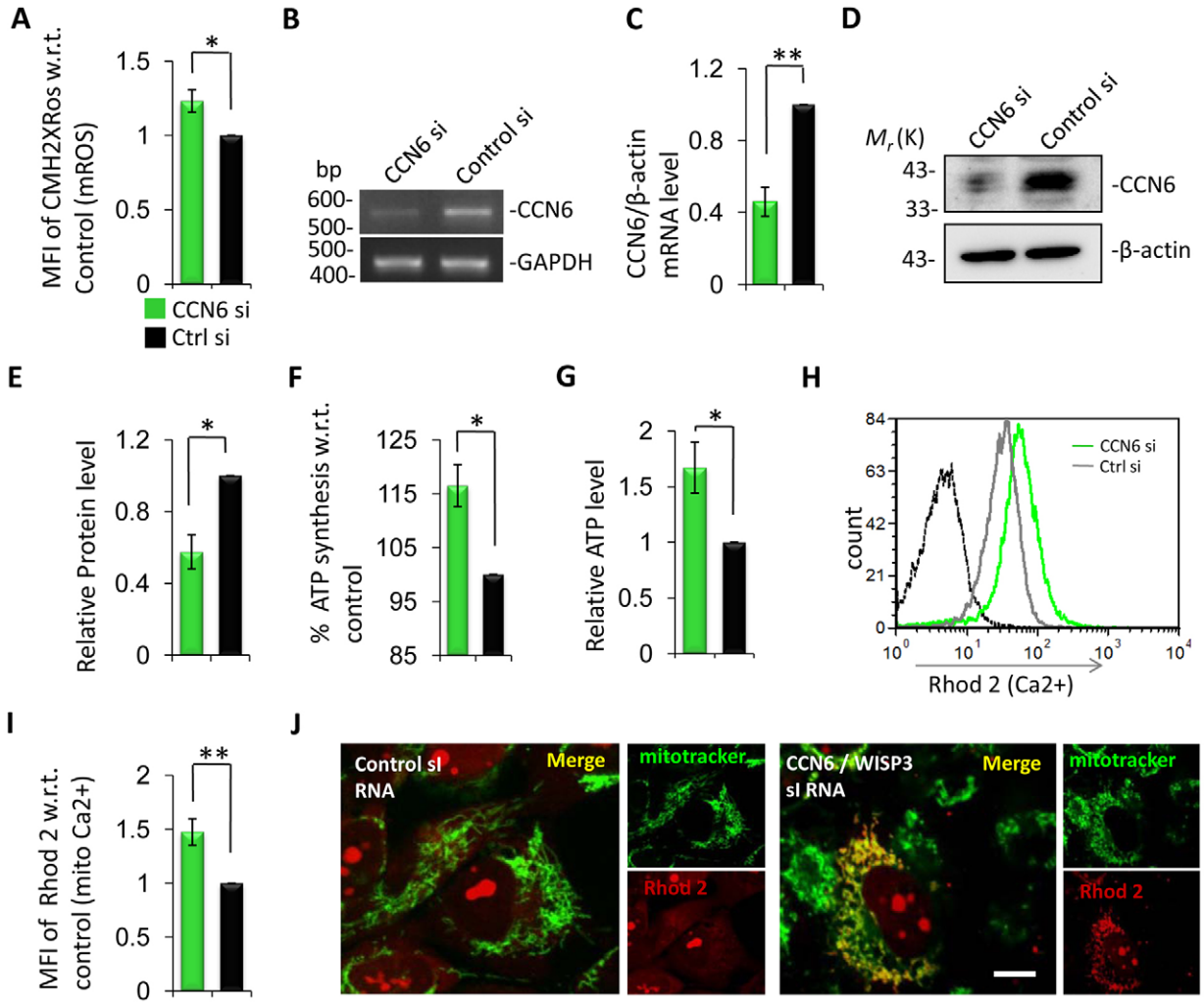

Fig. 1. Mitochondrial Ca^{2+}, ATP and ROS are regulated by CCN6. (A) Mitochondrial ROS (mROS) of CCN6-siRNA- (CCN6 si) versus control-siRNA (Ctrl si)-transfected cells as measured by FACS using CMH_2XRos (specific probe for mROS) (*n*=3). CCN6 knockdown depleted ~60% of CCN6, both at the RNA level relative to GAPDH (B,C) and protein level relative to β-actin (D,E) (*n*=3). (F) ATP synthesis within isolated mitochondria of CCN6-knockdown cells is higher than the control, as measured by using a luminometer and an ATP determination kit (*n*=4). (G) Total ATP is higher in CCN6-knockdown cells (*n*=4). (H) Histogram of FACS data shows right shift of Rhod 2 fluorescence in CCN6-knockdown cells (green line) compared to control (gray line) and unstained cells (dashed line). (I) Ca^{2+} uptake (Rhod2-bound cells) was significantly increased in CCN6-knockdown cells (*n*=6). (J) Confocal microscopy analysis reveals higher mitochondrial Ca^{2+} uptake, estimated through colocalization of Ca^{2+} (Rhod2, red) with mitochondria (MitoTracker Green FM, green). Data are represented as mean±s.e.m.; **P*<0.05, ***P*<0.01 (unpaired Student's *t*-test); *n* represents the number of independent experiments. Key shown in A applies to all panels. MFI, mean fluorescence intensity. Scale bar: 10 µm.

the transfected cells (Fig. 1B–E). The increase in accumulated mitochondrial ROS in CCN6-depleted cells could be an outcome of electron leakage on account of increased ETC activity (Murphy, 2009). Increased mitochondrial basal metabolic output was additionally displayed in isolated mitochondrial fractions of CCN6-siRNA-transfected cells as an increased rate of ATP synthesis, as detected by luciferase activity (Fig. 1F). Mitochondrial ATP contributed, at least partly, to the twofold boost in the total cellular ATP levels of CCN6-depleted cells (Fig. 1G). Augmented mitochondrial ATP synthesis upon CCN6 depletion correlated with increased mitochondrial Ca^{2+} content, as judged by performing flow cytometry (Fig. 1H,I) and confocal microscopy (Fig. 1J). Increased mitochondrial Ca^{2+} in CCN6-depleted cells was validated through colocalization of Rhod 2 (Ca^{2+}) and MitoTracker Green (mitochondria) as detected with *z*-stack analysis (Movies 1, 2 and Fig. S1). CCN6-mediated regulation of mitochondrial ATP synthesis and Ca^{2+} content, as demonstrated here, indicates an important role for CCN6 in mitochondrial-Ca^{2+}-mediated matrix mineralization (Brighton and Hunt, 1978; Lehninger, 1970; Villa-Bellosta et al., 2013).

CCN6 regulates mitochondrial membrane potential

Increased mitochondrial ROS, ATP and Ca^{2+} levels in CCN6-depleted cells implies that CCN6 influences the activity of the mitochondrial ETC. Because the membrane potential of respiring mitochondria is a vital indicator of electron transport, we examined the mitochondrial membrane potential of CCN6-depleted cells as compared to that of the corresponding control cells, using both MitoTracker Red and Rhodamine 123. As evident from flow cytometry analysis, CCN6-siRNA-transfected cells harbored an increased proportion of MitoTracker-Red- and Rhodamine-123-sensitive respiring mitochondria as compared to the corresponding controls (Fig. 2A–C). The increase in mitochondrial membrane potential upon CCN6 depletion was

Journal of Cell Science (2016) 129, 2841-2851 doi:10.1242/jcs.186247

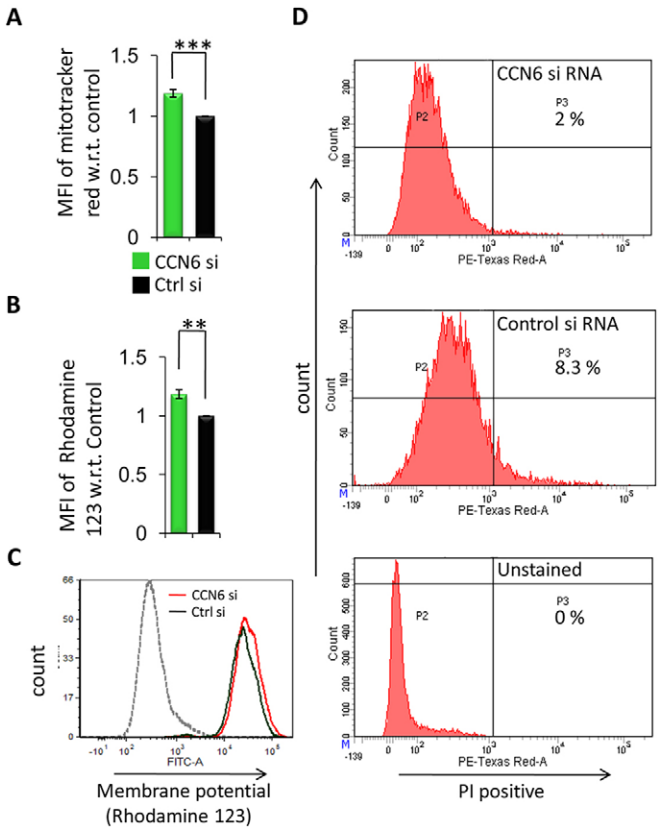

Fig. 2. CCN6-knockdown cells harbor more actively respiring mitochondria. (A) Flow cytometry analysis of cells loaded with MitoTracker Deep Red FM indicates that the amount of actively respiring mitochondria is significantly higher in CCN6-siRNA-transfected (CCN6 si) cells than in control scramble-siRNA-transfected (Ctrl si) cells (*n*=6). (B) Results of flow cytometry analysis using fluorescent probe Rhodamine 123, revealing a higher mitochondrial membrane potential of CCN6-siRNA-transfected cells compared to scramble-siRNA-transfected cells (*n*=3). (C) Histogram of Rhodamine 123 fluorescence (dashed line, unstained cells; red line, CCN6 siRNA; black line, scramble siRNA). (D) Propidium iodide (PI) exclusion assay. The propidium iodide exclusion assay was employed to measure dead cells both in CCN6-depleted and control cells (*n*=4). Data represent the percentage of the parent population – left quadrants (P2) are PI-negative (PE-Texas Red A channel) and right quadrants (P3) are PI-positive (PE-Texas Red A channel). Key shown in A also applies to B. MFI, mean fluorescence intensity. Data are represented as mean±s.e.m.; ***P*<0.01, ****P*<0.001 (unpaired Student's *t*-test); *n* represents the number of independent experiments.

modest enough to not cause any cell death as a result of necrosis or apoptosis, as assessed by both propidium iodide and annexin-V staining (Fig. 2D; Fig. S2A). The moderately increased membrane potential upon loss of CCN6 could be a reflection of a moderate increase in basal mitochondrial metabolism. Such augmentation in basal mitochondrial metabolism in CCN6-depleted cells might be conducive to protection from cell death, as demonstrated by the moderately improved survival in Fig. 2D. The effect of CCN6 depletion on cell proliferation was marginal (Fig. S2B).

Augmented mitochondrial ETC activity upon CCN6 depletion correlates with an increase in PGC1α expression and function

The transcriptional co-activator PGC1α [peroxisome-proliferator-activated receptor-γ coactivator-1α (PPARGC1A)] is inherently associated with mitochondrial function (Austin and St-Pierre, 2012; Spiegelman, 2007; Wenz, 2009). Thus, it was important to determine how increased mitochondrial ETC activity of CCN6-depleted cells correlates with PGC1α status. Accordingly, the PGC1α level in CCN6-siRNA-transfected cells was compared with that of controls. CCN6-depleted cells displayed increased levels of PGC1α both at the mRNA and protein levels (Fig. 3A,B). PGC1α expression has been previously correlated with increases in ROS (Austin and St-Pierre, 2012; Spiegelman, 2007; St-Pierre et al., 2006). Accordingly, we observed that the ROS quencher N-acetyl cysteine blocked the increase in PGC1α mRNA expression (Fig. 3C), suggesting that the increase in PGC1α expression in CCN6-depleted cells is ROS dependent. Elevated expression of the PGC1α-responsive oxidative phosphorylation (OXPHOS) gene *ATP5J* (Mootha et al., 2003) in CCN6-depleted cells, as demonstrated by both RT-PCR and immunoblot analyses, is furthermore suggestive of increased PGC1α function upon CCN6 depletion (Fig. 3D,E). Fig. 3F depicts the substantially increased levels of PGC1α and ATP5J protein in CCN6-depleted cells as compared to controls. Taken together, these results indicate that the elevated ROS levels that are, at least partly, contributed by augmented ETC activity might lead to increased PGC1α expression and function in CCN6-depleted cells. Considering the functional association of PGC1α with mitochondrial mass, we further checked for changes in mitochondrial mass in CCN6-siRNA-transfected cells by performing flow cytometry using MitoTracker Green. There was a consistent increase in mitochondrial mass in CCN6-siRNA-transfected cells compared to the corresponding controls (Fig. 3G). The increase in the intensity of MitoTracker Green of CCN6-siRNA-transfected cells was similar to the observed increase in the intensity of MitoTracker Red staining (Fig. 2A), indicating that CCN6 depletion increases the mass of respiring mitochondria (Zhou et al., 2011).

CCN6 is associated with mitochondria

In view of our experimental findings implicating CCN6 as a regulator of basal mitochondrial metabolism, it was necessary to check if CCN6 at least partially localizes to mitochondria. As depicted in Fig. 4A, subcellular fractionation of C-28/I2 cells followed by immunoblotting demonstrated the presence of CCN6 in mitochondrial fractions. COX-IV was used as a mitochondrial marker in these studies (Dolga et al., 2014). Proteinase K treatment of mitoplast preparations (Mick et al., 2012) and immunoblotting with antibodies to mitochondrial inner compartment marker proteins (NDUFS1 and ATP5A1) furthermore indicated that, although a considerable fraction of the CCN6 protein was accessible for proteinase K digestion, a notable fraction also remained resistant to it (Fig. 4B). Moreover, immunoblotting of the mitochondrial pellet and supernatant fractions, prepared separately from CCN6–Myc overexpressing cells in carbonate buffer (Mick et al., 2012; Zhou et al., 2008), with antibodies against Myc, Hsp60 (inner membrane and matrix marker) and TOM20 (outer membrane marker) indicated that, although most of the mitochondrial CCN6 was associated with the membrane, a portion was also present in the soluble fraction (De Vos et al., 2012; Sun et al., 2006) (Fig. 4C). Mitochondrial localization of CCN6 was also demonstrated through colocalization of endogenous, as well as overexpressed, CCN6 with MitoTracker Green by performing confocal microscopy (Fig. 4D). The extent of MitoTracker-Green–CCN6 colocalization, both at the endogenous level and after CCN6–Myc overexpression, was estimated by using a red, green and blue (RGB) profile plot (Fig. 4E endogenous CCN6, Fig. 4F overexpressed CCN6–Myc) and Pearson's coefficient (Fig. 4G).

Journal of Cell Science (2016) 129, 2841-2851 doi:10.1242/jcs.186247

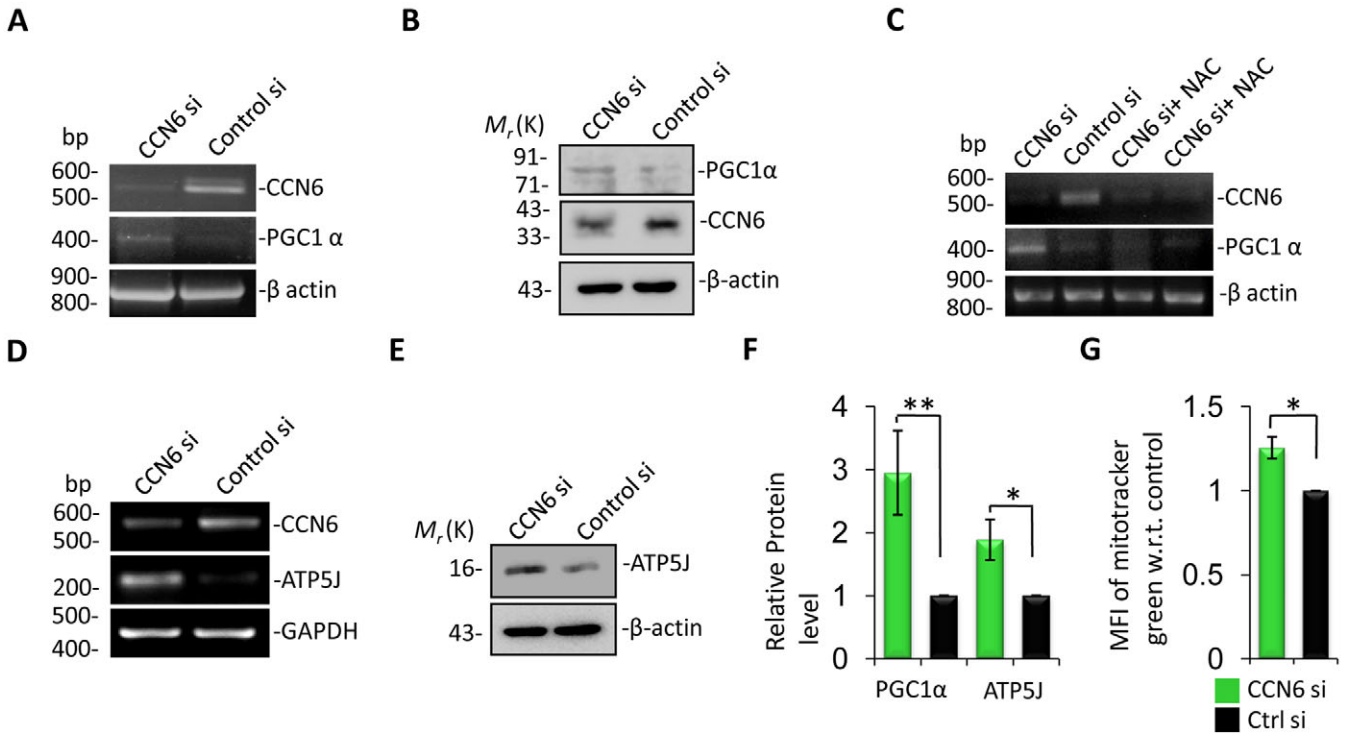

Fig. 3. Increased PGC1α expression and/or function in CCN6-knockdown cells, which is concomitant with an increase in mitochondrial content, is ROS dependent. Knockdown of CCN6 (CCN6 si) (~60% efficiency) with siRNA enhances PGC1α expression at the mRNA level (A) and protein level (B) (more than twofold). Control si, scramble control siRNA. (C) Treatment of CCN6-knockdown cells with ROS quencher N-acetyl cysteine (NAC) for 10 h reduced PGC1α expression level to baseline. An increase in PGC1α expression upon silencing of CCN6 increased expression of the PGC1α-responsive oxidative phosphorylation gene *ATP5J* at the RNA level (more than threefold) (D) and protein level (~threefold) (E). (F) Densitometry analysis of immunoblots reveals that PGC1α (*n*=4) and ATP5J (*n*=3) protein levels relative to β-actin were significantly higher in CCN6-knockdown cells than in control. (G) Flow cytometric analysis of MitoTracker green fluorescence in CCN6-knockdown C-28/I2 cells with respect to control (*n*=3). MFI, mean fluorescence intensity. *n* represents the number of independent experiments. Data are represented as mean±s.e.m.; **P*<0.05, ***P*<0.01 (unpaired Student's *t*-test).

Negative-control experiments for assessment of colocalization by using Pearson's coefficient were performed using isotype antibody and empty-vector-transfected cells (Fig. S3A,B). Presence of CCN6 in mitochondria was additionally substantiated by performing *z*-stacking analysis with confocal microscopy (Movie 3). These results suggest that the augmented ETC activity of CCN6-depleted cells might arise, at least partly, because of a lack of physical association of CCN6 with mitochondrial components. CCN6 might influence the activity of mitochondrial ETC components through intermolecular interactions, on account of the multimodular architecture of CCN6 (Engel, 2004; Hurvitz et al., 1999).

CCN6-depleted cells have altered mitochondrial morphology

Considering that CCN6 associates with mitochondria and that its depletion causes an increase in mitochondrial ETC activity and mass, it was important to examine whether CCN6 depletion correlates with altered mitochondrial morphology. Accordingly, transmission electron microscopy (TEM) analysis was performed, following similar procedures to those previously described (Pasqua et al., 2015), to evaluate the mitochondria of both CCN6-siRNA-transfected cells and the corresponding controls. TEM revealed an increased number of mitochondria together with elevated mitochondrial and cristae volume density {cristae volume density (%) = [sum of cristae area (μm^2) / mitochondrial area (μm^2)] × 100}, as well as crista area, in CCN6-depleted cells (Fig. 5A–H) as compared to controls. The red arrows in Fig. 5I indicate a possible site of mitochondrial fission in CCN6-depleted cells. The closer physical association of ER and mitochondria in CCN6-depleted cells as compared to controls (~27 nm vs ~52 nm) corroborates the observed mitochondrial Ca^{2+} influx that accompanies ATP synthesis (Fig. 5I–K). Alteration of mitochondrial shape and mass was furthermore evident upon depletion of CCN6 by using the CRISPR–Cas9 technique (Fig. S4). The efficiency of CCN6 depletion was demonstrated by using the SURVEYOR assay (Fig. S4C). The appearance of such features could correlate with the expression of chondrocyte hypertrophy markers, such as collagen X, which are associated with CCN6 depletion (Repudi et al., 2013). It will be interesting to investigate how CCN6 expression and mitochondrial morphology correlate with other cellular transformations that accompany hypertrophic differentiation (Buckwalter et al., 1986; Goldring et al., 2006).

Nrf2 regulates CCN6 expression

Given that CCN6 bears the potential to regulate mitochondrial respiration and ATP synthesis, it was important to understand how CCN6 itself is regulated. Previously, we have documented that CCN6 expression is enhanced by very low doses of ROS (Repudi et al., 2013). For an in-depth understanding of regulation of CCN6 expression, a bioinformatic approach was taken. Analysis of 10,000 bp upstream and downstream of the transcription start site revealed a binding site for the Nrf2 [nuclear factor erythroid 2 (NF-E2)-related factor 2 (NFE2L2)] transcription factor 4778 bp upstream of the transcription start site (Fig. 6A). Binding of Nrf2 to the region of the CCN6 promoter (designated Nrf2-binding site) identified by our bioinformatic search was confirmed by the

Journal of Cell Science (2016) 129, 2841-2851 doi:10.1242/jcs.186247

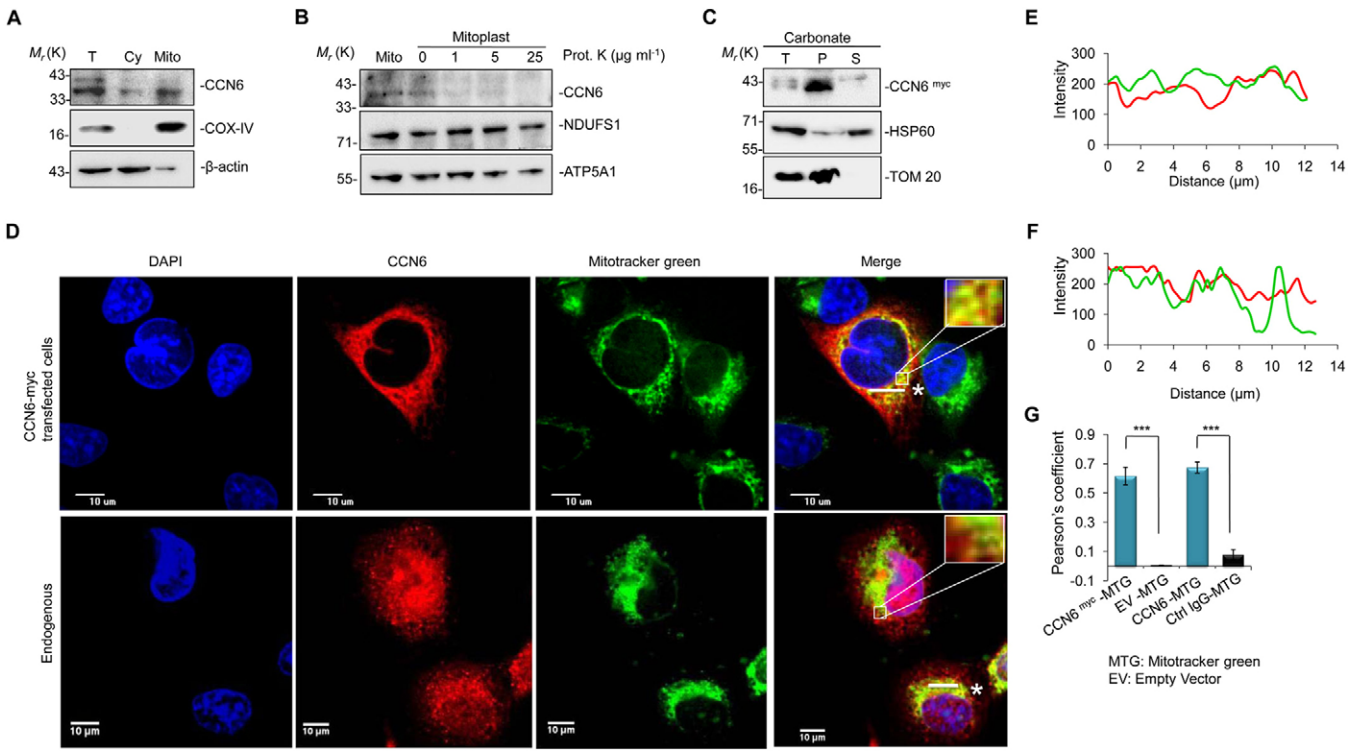

Fig. 4. CCN6 localizes to mitochondria. (A) Immunoblot demonstrating the presence of CCN6 in the mitochondrial fraction (Mito), cytosolic fraction (Cy) and whole-cell lysate (T) of C-28/I2 cells. COX-IV and β-actin were used as mitochondrial and cytosolic fraction loading controls, respectively. (B) Mitochondria from C-28/I2 cells were subjected to osmotic rupture for mitoplast preparation. Immunoblot of proteinase-K-digested (Prot. K) mitoplast corroborated localization of CCN6, which was associated with mitochondria. NDUFS1 and ATP5A1 were used as mitochondrial inner-compartment markers. (C) Immunoblot of a Na_2CO_3 (pH 11.5) preparation of isolated mitochondria from CCN6–Myc-transfected HEK293 cells, represented as total (T), membrane-rich pellet (P) and supernatant (S). TOM20 and HSP60 were used as references for mitochondrial outer membrane and mitochondrial inner membrane and matrix, respectively. (D) Confocal microscopy of C-28/I2 cells (endogenous) and CCN6–Myc-transfected C-28/I2 cells revealed colocalization of mitochondria (MitoTracker Green FM, green) with CCN6 (red). (E,F) RGB intensity plots of mitochondria (MitoTracker Green FM, green) and CCN6 (red) in C-28/I2 cells (endogenous, E; transfected with CCN6–Myc, F) depicting CCN6 localization in mitochondria. (G) Pearson's coefficient of colocalization between MitoTracker Green (MTG) and CCN6 was calculated from the confocal microscope data represented in panel D and Fig. S3. In calculating Pearson's coefficient for endogenous CCN6 (red) and MTG (green), confocal images of control IgG for CCN6 and MTG (Fig. S3A) were used as control. For calculation of Pearson's coefficient of colocalization in CCN6–Myc-transfected cells, confocal images of empty vector (EV)-transfected cells (Fig. S3B) were used as control (n=4). n represents the number of independent experiments. One way ANOVA followed by Bonferroni post-hoc test was performed to calculate the statistical significance of Pearson's coefficient; data are represented as mean±s.e.m., ***P<0.001.

luciferase activity of C-28/I2 cells that had been transfected with a luciferase reporter plasmid bearing the CCN6 promoter. In the presence of increasing concentrations of tert-butylhydroquinone (tBHQ), which promotes nuclear localization of Nrf2 (Nguyen et al., 2005), the reporter-plasmid-transfected C-28/I2 cells displayed progressively decreasing levels of luciferase activity, indicating that Nrf2 represses CCN6 expression (Fig. 6B). Nuclear translocation of Nrf2 upon tBHQ treatment and the concomitant decrease in CCN6 expression was substantiated separately using C-28/I2 cells (Fig. 6C,D). A chromatin immunoprecipitation (ChIP) assay further validated the binding of Nrf2 to the CCN6 promoter (Fig. 6E, top row). A similar ChIP assay that showed binding of RNA polymerase II (Fig. 6E, bottom row) established that the identified region was transcriptionally active. Interestingly, depletion of Nrf2 in chondrocytes through siRNA transfection led to an increase in CCN6 expression, both at the mRNA and protein levels, thus supporting that CCN6 expression is inhibited by Nrf2 (Fig. 6F,G). Considering that Nrf2 is a promoter of mitochondrial metabolism (Holmstrom et al., 2013; Ludtmann et al., 2014; Piantadosi et al., 2008), existence of a counter-regulatory CCN6–Nrf2 association that would appropriately control mitochondrial function seems plausible.

DISCUSSION

The involvement of CCN6 as an important player in mitochondrial respiration, Ca^{2+} accumulation and ATP synthesis brings a new dimension to our understanding of not only CCN6 function but also mitochondrial electron transport. The increased crista area and mitochondrial volume density along with closer mitochondria–ER association in CCN6-depleted cells as revealed by performing transmission electron microscopy (Fig. 5) are clearly indicative of an inverse relationship of mitochondrial metabolism and Ca^{2+} accumulation with CCN6 expression (Bravo et al., 2011; Rizzuto et al., 2009; Zampese et al., 2011). In view of the need of respiring mitochondria for release of mitochondrial Ca^{2+} during cell matrix mineralization (Brighton and Hunt, 1978; Lehninger, 1970; Villa-Bellosta et al., 2013), one can thus logically stipulate an important role of CCN6 in the regulation of mitochondrial electron transport and cell matrix calcification.

Mitochondrial localization of CCN6 and increased mitochondrial ATP synthesis in CCN6-depleted cells suggests that CCN6 could act as a brake for mitochondrial metabolism, thereby regulating cell growth. The regulation of ETC activity and its influence on cell growth and differentiation, although fundamental to biological systems, are far from being resolved. The potential involvement of

Journal of Cell Science (2016) 129, 2841-2851 doi:10.1242/jcs.186247

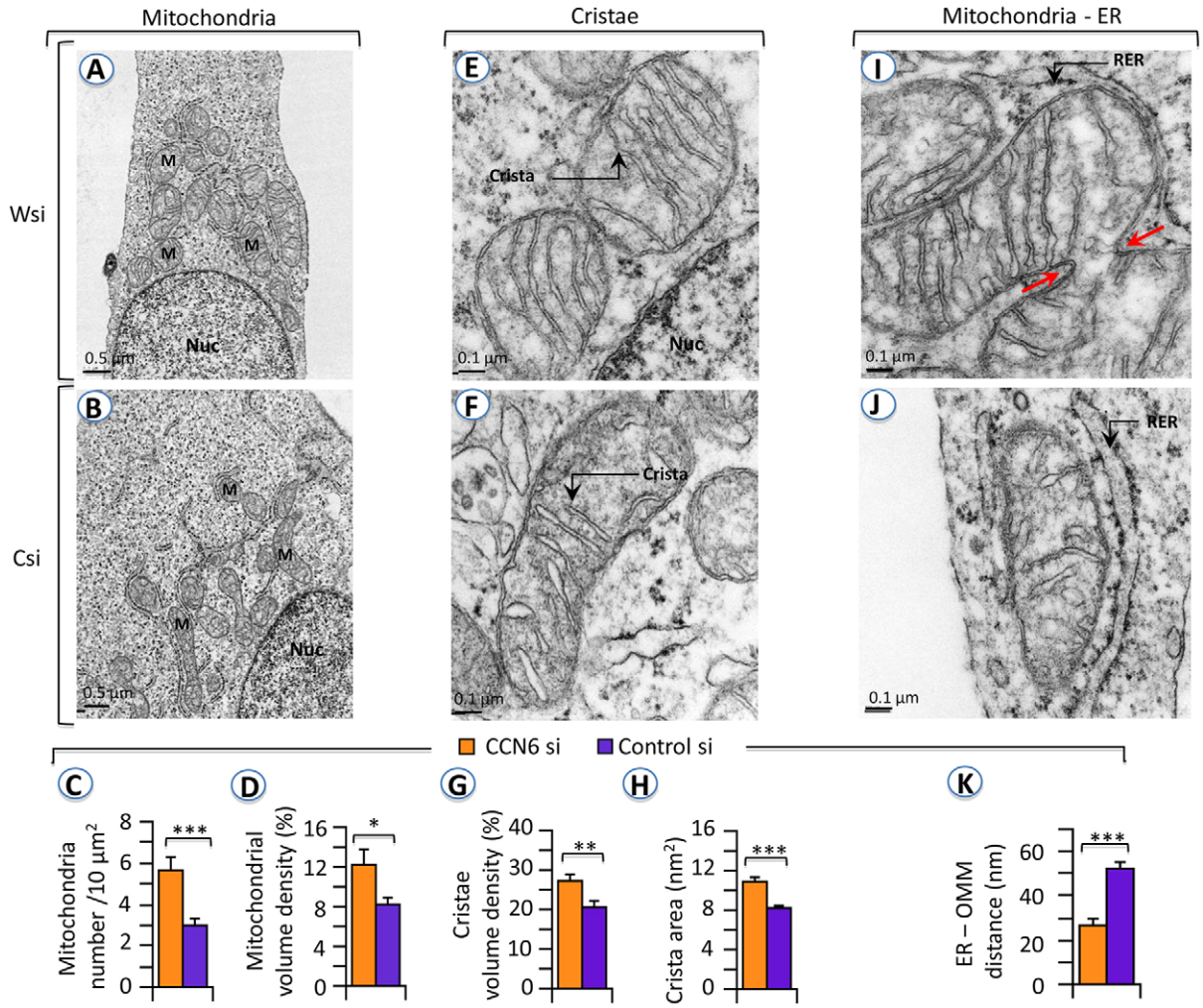

Fig. 5. Electron microscopy data showing mitochondrial morphology and ER–mitochondria juxtaposition in CCN6-knockdown vs control cells. Low magnification (2500×) electron microscopy images of CCN6 knockdown (Wsi, CCN6 si) (A) and control (Csi, control si) (B) cells. Morphometric analyses (*n*=25) show increased mitochondrial number (C) in Wsi cells and mitochondrial volume density (D) in Wsi cells compared to Csi cells. High magnification (15,000×) images of mitochondria in Wsi (E) and Csi (F). Morphometric analyses (*n*=100) show increased cristae volume density (G) and crista area (H) in Wsi cells compared to Csi cells. High magnification (15,000×) images of mitochondria and rough endoplasmic reticulum (RER) in Wsi (I) and Csi (J) cells showing the distance between mitochondria and ER. Morphometric analyses (*n*=25) revealed closer association of mitochondria and ER in Wsi cells to compared to in Csi cells (K). M, mitochondrion; Nuc, nucleus. Red arrows point to possible cleavage of mitochondria before complete fission. Data are represented as mean±s.e.m.; **P*<0.05, ***P*<0.01; ****P*<0.001 (unpaired Student's *t*-test with Welch's correction). *n* represents number of cells.

CCN6 therein could help to resolve the complex paradigm. In light of its multi-modular nature, CCN6 harbors an intrinsic potential for intermolecular interactions with other proteins. Therefore, it will be important to investigate whether the inhibitory influence of CCN6 on mitochondrial function is on account of its interactions with mitochondrial proteins. At the same time, it will be important to decipher if CCN6 uses any mitochondrial target sequence for mitochondrial entry or whether it is imported to mitochondria through an indirect mechanism (Doyle et al., 2013).

The present study demonstrates, for the first time, that the expression and function of PGC1α, the transcriptional co-activator that is essential for mitochondrial metabolism (Austin and St-Pierre, 2012; Spiegelman, 2007; Wenz, 2009), is modulated by the magnitude of CCN6-mediated effects on electron transport. PGC1α expression might be induced by the increased accumulation of ROS that results from augmented ETC activity in the absence of a fully functional CCN6 protein. Accumulated ROS perhaps promote the binding of CREB, MEF2, ATF2 and Foxo1 onto the PGC1α promoter (Fernandez-Marcos and Auwerx, 2011). PGC1α, once induced, could facilitate mitochondrial metabolism in a feed-forward mode. Thus, in the absence of a functional CCN6 protein, PGC1α could promote untimely cellular growth and hypertrophy through increased mitochondrial metabolism. The increased number and mass of mitochondria observed in CCN6-depleted cells (Figs 3G and 5C; Fig. S4F) could be partly facilitated by elevated PGC1α activity (Wu et al., 1999).

The documented inhibition of CCN6 expression by Nrf2 ushers in a new layer of coordination of mitochondrial dynamics through transcriptional regulation. CCN6 acts like a brake on ETC activity and ATP synthesis, whereas Nrf2, which is a facilitator of mitochondrial metabolism (Holmstrom et al., 2013; Ludtmann et al., 2014; Piantadosi et al., 2008), possibly coordinates with CCN6 by repressing its expression. The transcriptional co-activator PGC1α, which is turned on by accumulated ROS from enhanced ETC activity in a muted-CCN6 background, might be able to promote expression of Nrf2 through its influence on Notch

Journal of Cell Science (2016) 129, 2841-2851 doi:10.1242/jcs.186247

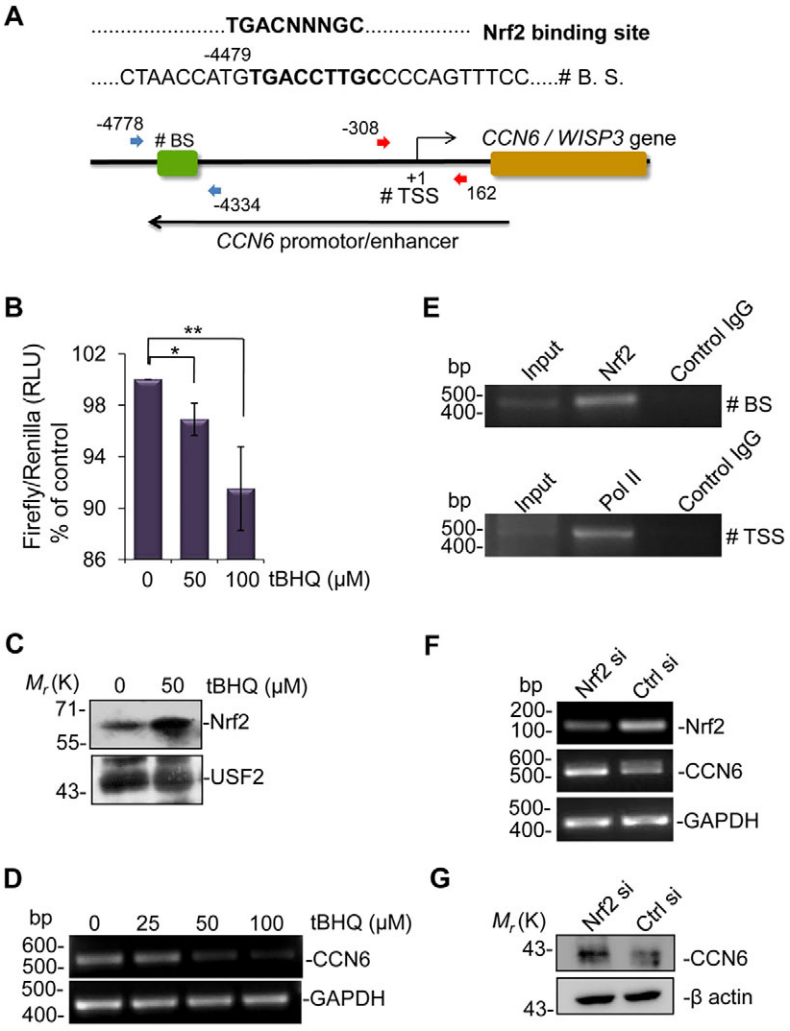

Fig. 6. Nrf2 binds to the CCN6 promotor and inhibits CCN6 expression. (A) The CCN6 promotor contains an Nrf2-binding site called anti-oxidant response element (ARE) represented as #B.S (Nrf2-binding site). N represents any nucleotide. (B) CCN6^{ARE}–Luc- and *Renilla*-co-transfected C-28/I2 cells that had been treated with the indicated concentration of tBHQ for 10 h showed a nuclear Nrf2-induced decrease in luciferase reporter activity. Treatment of C-28/I2 cells with indicated doses of tBHQ for 10 h enhanced Nrf2 nuclear translocation (~twofold) (C) and inhibited CCN6 expression (60% and 75% inhibition at 50 and 100 μM tBHQ, respectively; calculated using densitometry analysis with ImageJ) (D). USF2 was used as a nuclear loading control (C). (E) A ChIP assay confirmed Nrf2 binding to the CCN6 promotor (#BS) and RNA polymerase II (Pol II) binding to the transcription start site (#TSS). In Nrf2-knockdown cells (Nrf2 si) (~55% efficiency of knockdown), CCN6 expression was increased both at the RNA (~twofold) (F) and protein (~twofold) (G) levels. Data are represented as mean±s.e.m.; *P<0.05, **P<0.01 (unpaired Student's t-test); n=3 independent experiments. Ctrl si, control siRNA.

signaling (Sawada et al., 2014; Wakabayashi et al., 2014), and Nrf2 could repress CCN6 function furthermore.

The established link of CCN6 mutations with the development of the cartilage disease PPRD raises an important question. Given that CCN6 regulates mitochondrial respiration and ATP synthesis, why do specific phenotypes resulting from CCN6 mutations manifest primarily as loss of cartilage during puberty (Dalal et al., 2012; Ekbote et al., 2013; Garcia Segarra et al., 2012; Hurvitz et al., 1999; Liu et al., 2015; Luo et al., 2015; Yang et al., 2013)? Although it is true that the comprehension of CCN6-mutant phenotypes cannot be directly drawn through extrapolation of experimental findings related to wild-type CCN6, a clear knowledge of the function of the wild-type protein nevertheless could be required for a detailed analysis of the mutants. The functional significance of CCN6 expression at different developmental stages in different tissues is not clearly understood. But there is evidence that CCN6 plays an important role during cartilage growth and maintenance by sustaining expression of the extra cellular matrix (ECM) protein collagen II (Sen et al., 2004). Moreover, in view of the fact that CCN6 restricts mitochondrial metabolism, cartilage loss might result from premature chondrocyte hypertrophy that results from, at least in part, unregulated mitochondrial metabolism that is facilitated by a malfunctioning or nonfunctional CCN6 protein. Given that chondrocyte differentiation and ECM maintenance are crucial features of limb growth during puberty, cartilage could be most affected by mutant CCN6. A comprehensive characterization of the CCN6 protein and detailed evaluation of its significance in metabolic regulation and Ca^{2+} homeostasis could be useful in the functional analysis of PPRD-linked CCN6 mutants at the molecular level.

MATERIALS AND METHODS

Cell culture

C-28/I2 chondrocyte cells and HEK293 cells were maintained in Dulbecco's modified Eagle's medium (DMEM; Invitrogen) supplemented with 10% FBS, penicillin (1 unit ml^{-1}), streptomycin (1 μg ml^{-1}) and glutamine (2 mM) (Invitrogen) in a humidified incubator maintaining 37°C temperature and 5% CO_2 (Miller and Sen, 2007; Repudi et al., 2013). The C-28/I2 cell line was generated through retroviral infection of human juvenile costal cartilage with SV40 large T antigen (Goldring et al., 1994). The HEK293 cell line was purchased from American Type Culture Collection (ATCC). Both cell lines were tested for contamination.

Plasmids

Cloning of the CCN6 (WISP3) gene (GenBank AF100781) in between *Hind*III and *Xho*I restriction sites of the pSecTag2A vector to generate the CCN6–Myc construct has been described previously (Repudi et al., 2013). The Nrf2-binding site (anti-oxidant response element, ARE) between positions −4480 bp and −4471 bp was predicted upstream of CCN6 coding sequence from ensemble database. The sequence (−4492 bp to −4457 bp) was cloned between *Sal*I and *Bam*HI restriction enzyme sites in pGL3 luciferase vector to make the reporter construct (CCN6^{ARE}–Luc) (Repudi et al., 2013).

Journal of Cell Science (2016) 129, 2841-2851 doi:10.1242/jcs.186247

Transfection

The detailed transfection protocol has been reported previously (Repudi et al., 2013). Briefly, for plasmid expression studies, C-28/I2 chondrocyte cells were transfected with plasmid (2 µg) using Lipofectamine LTX transfection reagent (Invitrogen) and incubated for 48 h at 37°C in a humidified CO_2 cell culture incubator before harvesting for assays. For knockdown experiments, C-28/I2 chondrocyte cells were separately transfected with CCN6 siRNA (50 nM) or control siRNA (50 nM) (Dharmacon) and Nrf2 siRNA (25 nM) or control siRNA (25 nM) (Santa Cruz) using RNAiMAX transfection reagent (Invitrogen) as per the manufacturer's protocol and as described previously (Repudi et al., 2013). After 60–65 h of transfection, siRNA-transfected cells were analyzed.

RNA and cDNA preparation, and PCR

Total cellular RNA was isolated with the use of Trizol (Life Technologies) (Davis et al., 2006; Miller and Sen, 2007; Sen et al., 2004). The cDNA was prepared from RNA using cDNA synthesis kit (BioBharati Lifescience, India) as per the manufacturer's protocol. Gene expression was analyzed by performing PCR amplification of cDNA with specific primers: CCN6 (WISP3) forward 5′-ACCAAAGCTGGCTGGCAGTC-3′ and reverse 5′-TCTC CAGGTTCTCTGCAGTTTC-3′, GAPDH forward 5′-ACCACAGTCCATGCCATCAC-3′ and reverse 5′-TCCACCACCCTG TTGCTGTA-3′, PGC1α forward 5′-TGTGCTGCTCTGGTTGGTG-3′ and reverse 5′-GCTGAGTGTTGGCTGGTGC-3′, ATP5J forward 5′-GCACTTACCCTCCACTTCCT-3′ and reverse 5′-ATTCTTGCACTCAGTCCCGA-3′, β-actin forward 5′-ATCTGGCACCACA CCTTCTACAATGAGCTGCG-3′ and reverse 5′-CGTCATACTCCTGCTTGCTGATCC ACATCTGC-3′, and Nrf2 forward 5′-GAGAGCCCAGTCTTCATTGC-3′ and reverse 5′-TGCTCAATGTCCTGTTGCAT-3′.

Cell lysate preparation and immunoblotting

Whole-cell lysates were prepared using cell lysis buffer [20 mM Tris-HCl (pH 7.5), 500 mM NaCl, 1% Triton X-100, 1 mM EDTA, 50 mM dithiothreitol, 2 mM phenylmethylsulfonyl fluoride and 1% protease inhibitory cocktail (P8340, Sigma)] (Repudi et al., 2013). Total protein concentration was determined using the Bradford reagent (Bio-Rad). Subsequently, immunoblot analysis was performed by following a standard protocol (Repudi et al., 2013). Briefly, protein was transferred to PVDF membrane after SDS-PAGE and blocked for 2 h with either 5% BSA in TBST (Tris-buffered saline with 0.1% Tween-20) or 0.2% I-Block (Applied Biosystem). The blots were then incubated at 4°C overnight with separate primary antibodies using 1:1000 dilutions: anti-WISP3 (N-18) antibody (sc-8871, Santa Cruz) (Repudi et al., 2013; Tanaka et al., 2003), anti-PGC1α antibody (sc-13067, Santa Cruz) (Hong et al., 2011), anti-Nrf2 antibody (sc-13032, Santa Cruz) (Xiao et al., 2012), anti-USF2 antibody (sc-861, Santa Cruz) (Naskar et al., 2014), anti-ATP5A1 antibody (459240, Invitrogen), anti-COX-IV antibody (ab16056, Abcam), anti-NDUFS1 antibody (PA5-22309, Thermo Fisher), anti-HSP60 antibody (MA3-012, Thermo Fisher) and anti-ATP5J antibody (NBP1-88888, Novus Biologicals). Horseradish peroxidase (HRP)-conjugated secondary antibodies: anti-rabbit-IgG (A0545, Sigma), anti-mouse-IgG (A9044, Sigma) and anti-goat-IgG (A8919, Sigma) antibodies were used at a dilution 1:4000 for visualization with chemiluminescence reagent (Pierce and Millipore).

Subcellular fractionation

For isolation of mitochondria, C-28/I2 chondrocyte cells (6×10^8) were homogenized with a Dounce homogenizer in a buffer composed of 225 mM mannitol, 75 mM sucrose, 0.1 mM EGTA and 30 mM Tris-HCl (pH 7.4). Unbroken cells and nuclei were discarded by centrifuging the sample at 600 ***g*** for 5 min. Supernatant collected was further subjected to centrifugation at 7000 ***g*** for 10 min to obtain the mitochondrial pellet and cytosolic fraction. The mitochondrial pellet was washed with mitochondria wash buffer [225 mM mannitol, 75 mM sucrose and 30 mM Tris-HCl (pH 7.4)] and resuspended in mitochondrial resuspension buffer [250 mM mannitol, 0.5 mM EGTA and 5 mM HEPES (pH 7.4)] (Wieckowski et al., 2009).

To prepare nuclear and cytoplasmic extracts, C-28/I2 cells were incubated on ice in a hypotonic buffer [10 mM KCl, 1.5 mM $MgCl_2$, 10 mM HEPES (pH 7.9), 0.5 mM DTT, 1 mM PMSF and 1 mM Na_3VO_4] for 10 min. Cells were broken down with the addition of 0.5% NP-40. Centrifugation was carried out at 600 ***g*** for 5 min to obtain nuclear pellet and cytoplasmic supernatant. The nuclear pellet was sonicated in hypertonic buffer [1.5 mM $MgCl_2$, 420 mM NaCl, 20 mM HEPES (pH 7.9), 25% glycerol, 0.2 mM EDTA, 0.5 mM DTT, 1 mM PMSF, and 1 mM Na_3VO_4] for 15 s. Nuclear extract was obtained after centrifugation at 13,000 ***g*** for 15 min (Naskar et al., 2014).

Mitoplast preparation and mitochondrial fractionation with sodium carbonate buffer

Sub-mitochondrial localization of CCN6 was carried out by performing proteinase K protection assay. Mitochondria were osmotically ruptured by addition of MOPS buffer [10 mM MOPS and 1 mM EDTA, pH 7.2] to prepare mitoplasts (Mick et al., 2012). Mitoplast preparations of C-28/I2 cells were digested with increasing concentrations of proteinase K (1, 5 and 25 µg ml^{-1}). The effect of proteinase K digestion on mitoplast was blocked with 1 mM PMSF after 10–15 min of incubation on ice (Mick et al., 2012).

To isolate mitochondrial membranous and soluble sub-compartments, mitochondria from CCN6–Myc-transfected HEK293 cells were incubated for 30 min in carbonate buffer (100 mM Na_2CO_3, pH 11.5) and centrifuged for 45 min at 45,000 ***g*** (Mick et al., 2012; Zhou et al., 2008). The membranous part was mostly represented by a pellet, whereas the soluble part was represented by supernatant after centrifugation.

Flow cytometry

Total mitochondria, actively respiring mitochondria and membrane potential were measured by incubating cells for 20 min with 200 nM MitoTracker Green FM, Deep Red FM MitoTracker Red (Zhou et al., 2011) and Rhodamine 123 (Johnson et al., 1981) (Molecular Probes), respectively. Mitochondrial ROS (mROS) were analyzed by incubating cells with CMH_2XRos (200 nM) (Molecular Probes) for 25 min (Degli Esposti, 2002). Mitochondrial Ca^{2+} uptake was determined by treating cells with Rhod 2 (2 µM) (Molecular Probes) for 50 min (Hajnoczky et al., 1995; Mallilankaraman et al., 2012). Cells loaded with respective fluorescent dyes were trypsinized with 0.05% Trypsin EDTA (Invitrogen) and washed twice with PBS. The cells were finally resuspended in PBS at a concentration of 10^6 cells ml^{-1} and analyzed by using a BD FACS Calibur (BD Bioscience), taking 10,000 counts for each sample. For propidium iodide exclusion, siRNA-transfected C-28/I2 cells were trypsinized and washed with PBS. Propidium iodide solution (1 mg ml^{-1}) was added to cells before FACS analysis (Naskar et al., 2014). siRNA-transfected C-28/I2 cells were further analyzed for apoptosis or cell death by using an annexin-V–FITC and propidium iodide apoptosis detection kit (BD Biosciences), as per the manufacturer's protocol. To assess cell proliferation, C-28/I2 chondrocyte cells were incubated with carboxyfluorescein succinimidyl ester (CFSE) (5 µM) (Molecular Probes) for 20 min in PBS after 24 h of siRNA transfection (Lyons and Parish, 1994). CFSE fluorescence was measured after 65 h of siRNA transfection.

Measurement of mitochondrial ATP synthesis

Mitochondrial ATP synthesis was measured by incubating freshly prepared mitochondria (100 µg ml^{-1}) in respiration buffer [0.6 M sorbitol, 1 mM $MgCl_2$, 1 mM EDTA, 5 mM succinate, 1 mM ADP and 25 mM potassium phosphate pH 7.0] at 37°C for 15 min (Mittal et al., 2009; Mourier et al., 2014). Quantification of ATP was done by using an ATP determination kit (Molecular probes, Life Technologies) following the manufacturer's protocol. Luminescence for ATP measurement was recorded with a PerkinElmer VICTOR X3 luminometer.

Confocal microscopy

Confocal microscopy was performed using an Andor Revolution XD spinning disk microscope with an Andor ixon 897 EMCCD camera, and a Leica TCS SP8 microscope with PMT HyD detector. To check mitochondrial localization of CCN6 (WISP3), cells were first loaded with MitoTracker Green FM (200 nM) for 30 min, after which they were fixed with methanol, blocked with 2.5% BSA in PBS containing 0.1% Tween-20 (PBST) for 1 h, and incubated at 4°C overnight with either anti-WISP3

Journal of Cell Science

antibody (1:200) for localization in C-28/I2 cells or anti-Myc antibody (1:500) for localization in CCN6–Myc-transfected C-28/I2 chondrocytes. Cells were washed twice with PBST and incubated with secondary Alexa-Fluor-546-conjugated anti-goat antibody (1:2000) (Molecular Probes). DAPI was used to stain nucleus. For measurement of mitochondria-specific Ca^{2+} uptake, live-cell imaging was performed after treating the cells with MitoTracker Green FM (200 nM) for 30 min and Rhod 2 (μM) for 50 min (Hajnoczky et al., 1995; Mallilankaraman et al., 2012). Pearson's coefficient and RGB intensity plots of microscopy images for colocalization were performed using ImageJ (National Institutes of Health; NIH).

Electron microscopy

C-28/I2 chondrocyte cells were fixed with 2.5% glutaraldehyde and 2% paraformaldehyde in 0.15 M cacodylate buffer, and postfixed in 1% OsO_4 in 0.1 M cacodylate buffer for 1 h on ice. The cells were stained en bloc with 2–3% uranyl acetate for 1 h on ice. The cells were dehydrated in graded series of ethanol (20–100%) on ice followed by one wash with 100% ethanol and two washes with acetone (15 min each) and embedded with Durcupan. Sections were cut at 50 to 60 nm on a Leica UCT ultramicrotome, and picked up on Formvar and carbon-coated copper grids. Sections were stained with 2% uranyl acetate for 5 min and Sato's lead stain for 1 min. Grids were viewed using a JEOL 1200EX II (JEOL, Peabody, MA) transmission electron microscope and photographed using a Gatan digital camera (Gatan, Pleasanton, CA).

Morphometric analysis of mitochondria

Samples were anonymized, and morphometric measurements were made randomly from different cells as described previously (Pasqua et al., 2015). The line segment tool in NIH ImageJ 1.49 software was used to measure the distance between ER and mitochondria. The free-hand tool of the NIH ImageJ 1.49 software was used to manually trace around the cristae membrane, mitochondrial outer membrane area and cytoplasm area for determination of the mitochondrial and cristae volume density. The sum of the area of the total complement of cristae represented the cristae membrane surface area. To normalize the measurement, this sum was divided by the outer membrane area per mitochondrion. The sum of the area of the mitochondria was divided by the area of the cytoplasm and multiplied by 100 to determine the mitochondrial volume density (%). For determination of the cristae volume density (%), the sum of the area of the cristae was divided by the outer area of the mitochondria and multiplied by 100, as described previously (Pasqua et al., 2015). A 19×23-cm rectangular grid was overlaid on each image to count the number of mitochondria in each image, and the mitochondria number is presented per 10 μm^2 area of the cytoplasm.

Chromatin immunoprecipitation

The ChIP assay was performed by following standard protocols (Bernstein et al., 2005; Naskar et al., 2014). Briefly, C-28/I2 ($\sim 6\times10^6$) cells were incubated at 37°C for 10 min with 1% formaldehyde (Molecular Biology Grade, Calbiochem) to crosslink protein and DNA. Over-crosslinking was prevented with the addition of glycine to a final concentration 125 mM and incubation for 5 min. After lysis of cells in 1 ml SDS lysis buffer [50 mM Tris-Cl (pH-8.1), 10 mM EDTA and 1% SDS] sonication was performed to generate genomic DNA fragments of 100 bp to 500 bp in size. The sample was then diluted fivefold with ChIP dilution buffer [16.7 mM Tris-Cl (pH 8.1), 167 mM NaCl, 1.2 mM EDTA, 1.1% Triton X-100 and 1% SDS] and pre-cleared for 1 h with salmon sperm DNA and protein G agarose beads (Life Technologies). Subsequently, the sample was incubated overnight at 4°C with either 7 μg of anti-Nrf2 antibody (sc-13032X, Santa Cruz) or anti-RNA-polymerase-II antibody (sc-5943, Santa Cruz) (Naskar et al., 2014). In each case, rabbit IgG was used as control. The pulled down immune complex was sequentially washed with low-salt immune complex buffer (20 mM Tris-HCl, pH 8.1, 0.1% SDS, 1% Triton X-100, 150 mM NaCl), high-salt immune complex buffer (20 mM Tris-HCl, pH 8.1, 0.1% SDS, 1% Triton X-100, 500 mM NaCl), LiCl immune complex buffer (10 mM Tris-HCl, pH 8.1, 1 mM EDTA, 0.25 M LiCl, 1% deoxycholic acid, 1% Triton X-100) and Tris-EDTA (TE) buffer (10 mM Tris-HCl, pH 8.0, 1 mM EDTA). Reverse crosslinking was carried out by heating the sample with Chelex 100 (Bio-Rad) for 10 min on a dry bath. After proteinase K digestion, DNA from chromatin was purified by following standard phenol–chloroform extraction and isopropanol precipitation. Finally, the DNA was quantified by performing semi-quantitative PCR. Primers used were: ARE forward 5′-TCCTGCTACTGATCATGGTG-3′ and reverse 5′-AAGAGCTAACATTGGCCGA G-3′, and RNA polymerase II forward 5′-GCCTCCGAGAGAATCTGAG-3′ and reverse 5′-CTCTACCTCCCA-CACTACC-3′.

Luciferase assay

C-28/I2 cells were co-transfected with $CCN6^{ARE}$–Luc reporter construct and *Renilla* at a ratio of 50:1. After 48 h of transfection, cells were treated with 25, 50 and 100 μM of tBHQ for 6 h. The luciferase assay kit (Promega) was used to measure firefly and *Renilla* luciferase activity.

CCN6 CRISPR–Cas9 – C-28/I2 chondrocyte lines

High-quality guide RNA with a minimum of off-target effects and a high-quality score (89) was designed using CRISPR design tool (http://crispr.mit.edu) on all the exons of the CCN6 (WISP3) genomic region (RefSeq gene NG_011748.1). The guide RNA was cloned into pSpCas9 (BB) 2A-Puro vector (Addgene). The primer pair 5′-CACCGCCACGGTCCCAGCGACAT GC-3′ and 5′-AAACGCATGTCGCTGGGACCGTGGC-3′ was annealed, phosphorylated with polynucleotide kinase (Thermo Fisher) and ligated to the BbsI (Fermentus) digested vector using T7 ligase (NEB). The sequenced positive clone was used to transfect C-28/I2 cells using Lipofectamine LTX (Life Technologies). After 24–48 h of transfection cells, were subjected to puromycin selection (Ran et al., 2013). After 3–4 passages in growth medium without puromycin, cells were harvested for assays.

SURVEYOR assay

Insertion or deletion mutations in the genome were validated using SURVEYOR assay kit (IDT) (Ran et al., 2013). Isolated genomic DNA was subjected to PCR amplification using primer pair 5′-CTGCGAAGGC-AGGTTATTAG-3′ and 5′-GAAGCTCATGAACGAACACA-3′ flanking the target location. 400 ng of PCR products purified from wild-type C-28/I2 cells and CRISPR CCN6-knockout cells were melted and annealed in a buffer containing 10 mM Tris-HCl, pH-8.8, 50 mM KCl, 0.01% Tween-20 and 1.5 mM $MgCl_2$ to form a heteroduplex. The hybrid DNA was then incubated with 1 μl enhancer S, 1 μl nuclease S and 2 μl 0.15 M $MgCl_2$ at 42°C for 50 min as per the manufacturer's protocol. Cleaved products, which would arise only from heteroduplexes, were then analyzed in 2% agarose gel. Indel percentage was calculated by using the following the formula:

$$\text{Indel}\,(\%) = 100 \times [1 - \sqrt{\{1 - (b + c)/(a + b + c)\}}] \qquad (1)$$

(Ran et al., 2013).

In Eqn 1, a represents the band intensity of PCR product (529 bp) from nuclease-S-undigested duplex formed from genomic DNA of CCN6 WT cells and CRISPR CCN6 cells, whereas b and c represent the band intensities of nuclease-S-digested products of 211 bp and 318 bp, from the heteroduplex (529 bp), respectively.

Statistical analysis

GraphPad software was used for unpaired two-tailed Student's *t*-test analyses. Origin 8 software was employed for one way ANOVA followed by Bonferroni post-hoc test for comparison of Pearson's coefficients (DeGeer et al., 2015; Zhou et al., 2016). Data are represented as mean±s.e.m. Statistical significance was drawn by calculating *P*-values, which are represented as $*P<0.05$, $**P<0.01$ and $***P<0.001$.

Acknowledgements

We are grateful to Srinivasa Rao Repudi (The Hebrew University of Jerusalem, Jerusalem, Israel) for plasmids used in the study. We thank G. Ghosh, S. Kundu, S. Jati, S. N. Dey, T. Dalui and U. Ghosh for critical reading of the manuscript and useful comments. We thank D. Sarkar and S. Bhattacharya for help with confocal microscopy analysis. Transmission electron microscopy was conducted at the Cellular & Molecular Medicine Electron Microscopy core facility, University of California, San Diego.

Competing interests
The authors declare no competing or financial interests.

Author contributions
M.S. designed the research, organized experiments and wrote the paper. M.P. organized and performed experiments and helped in writing paper. S.K.M. performed TEM. D.K.P. performed some experiments.

Funding
This work is supported by a grant from the Department of Science and Technology, Ministry of Science and Technology [grant number SB/SO/BB-016/2014]; and institutional funding [grant number BSC0120]. M.P. and D.K.P. are supported by the Council of Scientific and Industrial Research (CSIR) fellowships, Government of India. A research career scientist award from the U.S. Department of Veterans Affairs supports S.K.M.

Supplementary information
Supplementary information available online at
http://jcs.biologists.org/lookup/suppl/doi:10.1242/jcs.186247/-/DC1

References
Austin, S. and St-Pierre, J. (2012). PGC1alpha and mitochondrial metabolism–emerging concepts and relevance in ageing and neurodegenerative disorders. *J. Cell Sci.* **125**, 4963-4971.
Bernstein, B. E., Kamal, M., Lindblad-Toh, K., Bekiranov, S., Bailey, D. K., Huebert, D. J., McMahon, S., Karlsson, E. K., Kulbokas, E. J., III, Gingeras, T. R. et al. (2005). Genomic maps and comparative analysis of histone modifications in human and mouse. *Cell* **120**, 169-181.
Bravo, R., Vicencio, J. M., Parra, V., Troncoso, R., Munoz, J. P., Bui, M., Quiroga, C., Rodriguez, A. E., Verdejo, H. E., Ferreira, J. et al. (2011). Increased ER-mitochondrial coupling promotes mitochondrial respiration and bioenergetics during early phases of ER stress. *J. Cell Sci.* **124**, 2143-2152.
Brighton, C. T. and Hunt, R. M. (1978). The role of mitochondria in growth plate calcification as demonstrated in a rachitic model. *J. Bone Joint Surg. Am.* **60**, 630-639.
Brigstock, D. R., Goldschmeding, R., Katsube, K.-I., Lam, S. C.-T., Lau, L. F., Lyons, K., Naus, C., Perbal, B., Riser, B., Takigawa, M. et al. (2003). Proposal for a unified CCN nomenclature. *Mol. Pathol.* **56**, 127-128.
Brookes, P. S., Yoon, Y., Robotham, J. L., Anders, M. W. and Sheu, S.-S. (2004). Calcium, ATP, and ROS: a mitochondrial love-hate triangle. *Am. J. Physiol. Cell Physiol.* **287**, C817-C833.
Buckwalter, J. A., Mower, D., Ungar, R., Schaeffer, J. and Ginsberg, B. (1986). Morphometric analysis of chondrocyte hypertrophy. *J. Bone Joint Surg. Am.* **68**, 243-255.
Dalal, A., Bhavani, G. S. L., Togarrati, P. P., Bierhals, T., Nandineni, M. R., Danda, S., Danda, D., Shah, H., Vijayan, S., Gowrishankar, K. et al. (2012). Analysis of the WISP3 gene in Indian families with progressive pseudorheumatoid dysplasia. *Am. J. Med. Genet. A* **158A**, 2820-2828.
Davis, L., Chen, Y. and Sen, M. (2006). WISP-3 functions as a ligand and promotes superoxide dismutase activity. *Biochem. Biophys. Res. Commun.* **342**, 259-265.
De Vos, K. J., Morotz, G. M., Stoica, R., Tudor, E. L., Lau, K.-F., Ackerley, S., Warley, A., Shaw, C. E. and Miller, C. C. (2012). VAPB interacts with the mitochondrial protein PTPIP51 to regulate calcium homeostasis. *Hum. Mol. Genet.* **21**, 1299-1311.
DeGeer, J., Kaplan, A., Mattar, P., Morabito, M., Stochaj, U., Kennedy, T. E., Debant, A., Cayouette, M., Fournier, A. E. and Lamarche-Vane, N. (2015). Hsc70 chaperone activity underlies Trio GEF function in axon growth and guidance induced by netrin-1. *J. Cell Biol.* **210**, 817-832.
Degli Esposti, M. (2002). Measuring mitochondrial reactive oxygen species. *Methods* **26**, 335-340.
Dolga, A. M., de Andrade, A., Meissner, L., Knaus, H.-G., Höllerhage, M., Christophersen, P., Zischka, H., Plesnila, N., Höglinger, G. U. and Culmsee, C. (2014). Subcellular expression and neuroprotective effects of SK channels in human dopaminergic neurons. *Cell Death Dis.* **5**, e999.
Doyle, S. R., Kasinadhuni, N. R. P., Chan, C. K. and Grant, W. N. (2013). Evidence of evolutionary constraints that influences the sequence composition and diversity of mitochondrial matrix targeting signals. *PLoS ONE* **8**, e67938.
Ekbote, A. V., Danda, D., Kumar, S., Danda, S., Madhuri, V. and Gibikote, S. (2013). A descriptive analysis of 14 cases of progressive-psuedorheumatoid-arthropathy of childhood from south India: review of literature in comparison with juvenile idiopathic arthritis. *Semin. Arthritis Rheum.* **42**, 582-589.
Engel, J. (2004). Role of oligomerization domains in thrombospondins and other extracellular matrix proteins. *Int. J. Biochem. Cell Biol.* **36**, 997-1004.
Fernandez-Marcos, P. J. and Auwerx, J. (2011). Regulation of PGC-1alpha, a nodal regulator of mitochondrial biogenesis. *Am. J. Clin. Nutr.* **93**, 884S-890S.
Garcia Segarra, N., Mittaz, L., Campos-Xavier, A. B., Bartels, C. F., Tuysuz, B., Alanay, Y., Cimaz, R., Cormier-Daire, V., Di Rocco, M., Duba, H.-C. et al. (2012). The diagnostic challenge of progressive pseudorheumatoid dysplasia (PPRD): a review of clinical features, radiographic features, and WISP3 mutations in 63 affected individuals. *Am. J. Med. Genet. C Semin. Med. Genet.* **160C**, 217-229.
Goldring, M. B., Birkhead, J. R., Suen, L. F., Yamin, R., Mizuno, S., Glowacki, J., Arbiser, J. L. and Apperley, J. F. (1994). Interleukin-1 beta-modulated gene expression in immortalized human chondrocytes. *J. Clin. Invest.* **94**, 2307-2316.
Goldring, M. B., Tsuchimochi, K. and Ijiri, K. (2006). The control of chondrogenesis. *J. Cell. Biochem.* **97**, 33-44.
Hajnoczky, G., Robb-Gaspers, L. D., Seitz, M. B. and Thomas, A. P. (1995). Decoding of cytosolic calcium oscillations in the mitochondria. *Cell* **82**, 415-424.
Holmstrom, K. M., Baird, L., Zhang, Y., Hargreaves, I., Chalasani, A., Land, J. M., Stanyer, L., Yamamoto, M., Dinkova-Kostova, A. T. and Abramov, A. Y. (2013). Nrf2 impacts cellular bioenergetics by controlling substrate availability for mitochondrial respiration. *Biol. Open* **2**, 761-770.
Hong, T., Ning, J., Yang, X., Liu, H.-Y., Han, J., Liu, Z. and Cao, W. (2011). Fine-tuned regulation of the PGC-1alpha gene transcription by different intracellular signaling pathways. *Am. J. Physiol. Endocrinol. Metab.* **300**, E500-E507.
Hurvitz, J. R., Suwairi, W. M., Van Hul, W., El-Shanti, H., Superti-Furga, A., Roudier, J., Holderbaum, D., Pauli, R. M., Herd, J. K., Van Hul, E. V. et al. (1999). Mutations in the CCN gene family member WISP3 cause progressive pseudorheumatoid dysplasia. *Nat. Genet.* **23**, 94-98.
Johnson, L. V., Walsh, M. L., Bockus, B. J. and Chen, L. B. (1981). Monitoring of relative mitochondrial membrane potential in living cells by fluorescence microscopy. *J. Cell Biol.* **88**, 526-535.
Lehninger, A. L. (1970). Mitochondria and calcium ion transport. *Biochem. J.* **119**, 129-138.
Liu, L., Li, N., Zhao, Z., Li, W. and Xia, W. (2015). Novel WISP3 mutations causing spondyloepiphyseal dysplasia tarda with progressive arthropathy in two unrelated Chinese families. *Joint Bone Spine* **82**, 125-128.
Ludtmann, M. H. R., Angelova, P. R., Zhang, Y., Abramov, A. Y. and Dinkova-Kostova, A. T. (2014). Nrf2 affects the efficiency of mitochondrial fatty acid oxidation. *Biochem. J.* **457**, 415-424.
Luo, H., Shi, C., Mao, C., Jiang, C., Bao, D., Guo, J., Du, P., Wang, Y., Liu, Y., Liu, X. et al. (2015). A novel compound WISP3 mutation in a Chinese family with progressive pseudorheumatoid dysplasia. *Gene* **564**, 35-38.
Lyons, A. B. and Parish, C. R. (1994). Determination of lymphocyte division by flow cytometry. *J. Immunol. Methods* **171**, 131-137.
Mallilankaraman, K., Doonan, P., Cárdenas, C., Chandramoorthy, H. C., Müller, M., Miller, R., Hoffman, N. E., Gandhirajan, R. K., Molgó, J., Birnbaum, M. J. et al. (2012). MICU1 is an essential gatekeeper for MCU-mediated mitochondrial Ca(2+) uptake that regulates cell survival. *Cell* **151**, 630-644.
Mick, D. U., Dennerlein, S., Wiese, H., Reinhold, R., Pacheu-Grau, D., Lorenzi, I., Sasarman, F., Weraarpachai, W., Shoubridge, E. A., Warscheid, B. et al. (2012). MITRAC links mitochondrial protein translocation to respiratory-chain assembly and translational regulation. *Cell* **151**, 1528-1541.
Miller, D. S. and Sen, M. (2007). Potential role of WISP3 (CCN6) in regulating the accumulation of reactive oxygen species. *Biochem. Biophys. Res. Commun.* **355**, 156-161.
Mittal, N., Babu, M. M. and Roy, N. (2009). The efficiency of mitochondrial electron transport chain is increased in the long-lived mrg19 Saccharomyces cerevisiae. *Aging Cell* **8**, 643-653.
Mootha, V. K., Lindgren, C. M., Eriksson, K.-F., Subramanian, A., Sihag, S., Lehar, J., Puigserver, P., Carlsson, E., Ridderstråle, M., Laurila, E. et al. (2003). PGC-1alpha-responsive genes involved in oxidative phosphorylation are coordinately downregulated in human diabetes. *Nat. Genet.* **34**, 267-273.
Mourier, A., Ruzzenente, B., Brandt, T., Kuhlbrandt, W. and Larsson, N.-G. (2014). Loss of LRPPRC causes ATP synthase deficiency. *Hum. Mol. Genet.* **23**, 2580-2592.
Murphy, M. P. (2009). How mitochondria produce reactive oxygen species. *Biochem. J.* **417**, 1-13.
Naskar, D., Maiti, G., Chakraborty, A., Roy, A., Chattopadhyay, D. and Sen, M. (2014). Wnt5a-Rac1-NF-kappaB homeostatic circuitry sustains innate immune functions in macrophages. *J. Immunol.* **192**, 4386-4397.
Nguyen, T., Sherratt, P. J., Nioi, P., Yang, C. S. and Pickett, C. B. (2005). Nrf2 controls constitutive and inducible expression of ARE-driven genes through a dynamic pathway involving nucleocytoplasmic shuttling by Keap1. *J. Biol. Chem.* **280**, 32485-32492.
Pal, A., Huang, W., Li, X., Toy, K. A., Nikolovska-Coleska, Z. and Kleer, C. G. (2012). CCN6 modulates BMP signaling via the Smad-independent TAK1/p38 pathway, acting to suppress metastasis of breast cancer. *Cancer Res.* **72**, 4818-4828.
Pasqua, T., Mahata, S., Bandyopadhyay, G. K., Biswas, A., Perkins, G. A., Sinha Hikim, A. P., Goldstein, D. S., Eiden, L. E. and Mahata, S. K. (2015). Impact of Chromogranin A deficiency on catecholamine storage, catecholamine granule morphology, and chromaffin cell energy metabolism in vivo. *Cell Tissue Res.* **363**, 693-712.
Pennica, D., Swanson, T. A., Welsh, J. W., Roy, M. A., Lawrence, D. A., Lee, J., Brush, J., Taneyhill, L. A., Deuel, B., Lew, M. et al. (1998). WISP genes are members of the connective tissue growth factor family that are up-regulated in wnt-

1-transformed cells and aberrantly expressed in human colon tumors. *Proc. Natl. Acad. Sci. USA* **95**, 14717-14722.

Perbal, B. (2013). CCN proteins: a centralized communication network. *J. Cell Commun. Signal.* **7**, 169-177.

Piantadosi, C. A., Carraway, M. S., Babiker, A. and Suliman, H. B. (2008). Heme oxygenase-1 regulates cardiac mitochondrial biogenesis via Nrf2-mediated transcriptional control of nuclear respiratory factor-1. *Circ. Res.* **103**, 1232-1240.

Ran, F. A., Hsu, P. D., Wright, J., Agarwala, V., Scott, D. A. and Zhang, F. (2013). Genome engineering using the CRISPR-Cas9 system. *Nat. Protoc.* **8**, 2281-2308.

Repudi, S. R., Patra, M. and Sen, M. (2013). WISP3-IGF1 interaction regulates chondrocyte hypertrophy. *J. Cell Sci.* **126**, 1650-1658.

Rizzuto, R., Marchi, S., Bonora, M., Aguiari, P., Bononi, A., De Stefani, D., Giorgi, C., Leo, S., Rimessi, A., Siviero, R. et al. (2009). Ca(2+) transfer from the ER to mitochondria: when, how and why. *Biochim. Biophys. Acta* **1787**, 1342-1351.

Sawada, N., Jiang, A., Takizawa, F., Safdar, A., Manika, A., Tesmenitsky, Y., Kang, K.-T., Bischoff, J., Kalwa, H., Sartoretto, J. L. et al. (2014). Endothelial PGC-1alpha mediates vascular dysfunction in diabetes. *Cell Metab.* **19**, 246-258.

Sen, M., Cheng, Y.-H., Goldring, M. B., Lotz, M. K. and Carson, D. A. (2004). WISP3-dependent regulation of type II collagen and aggrecan production in chondrocytes. *Arthritis Rheum.* **50**, 488-497.

Spiegelman, B. M. (2007). Transcriptional control of mitochondrial energy metabolism through the PGC1 coactivators. *Novartis Found Symp.* **287**, 60-63; discussion 63-69.

St-Pierre, J., Drori, S., Uldry, M., Silvaggi, J. M., Rhee, J., Jäger, S., Handschin, C., Zheng, K., Lin, J., Yang, W. et al. (2006). Suppression of reactive oxygen species and neurodegeneration by the PGC-1 transcriptional coactivators. *Cell* **127**, 397-408.

Sun, F.-C., Wei, S., Li, C.-W., Chang, Y.-S., Chao, C.-C. and Lai, Y.-K. (2006). Localization of GRP78 to mitochondria under the unfolded protein response. *Biochem. J.* **396**, 31-39.

Tanaka, S., Sugimachi, K., Maehara, S.-I., Shimada, M. and Maehara, Y. (2003). A loss of function mutation in WISP3 derived from microsatellite unstable gastric carcinoma. *Gastroenterology* **125**, 1563-1564.

Villa-Bellosta, R., Rivera-Torres, J., Osorio, F. G., Acin-Perez, R., Enriquez, J. A., Lopez-Otin, C. and Andres, V. (2013). Defective extracellular pyrophosphate metabolism promotes vascular calcification in a mouse model of Hutchinson-Gilford progeria syndrome that is ameliorated on pyrophosphate treatment. *Circulation* **127**, 2442-2451.

Wakabayashi, N., Skoko, J. J., Chartoumpekis, D. V., Kimura, S., Slocum, S. L., Noda, K., Palliyaguru, D. L., Fujimuro, M., Boley, P. A., Tanaka, Y. et al. (2014). Notch-Nrf2 axis: regulation of Nrf2 gene expression and cytoprotection by notch signaling. *Mol. Cell. Biol.* **34**, 653-663.

Wenz, T. (2009). PGC-1alpha activation as a therapeutic approach in mitochondrial disease. *IUBMB Life* **61**, 1051-1062.

Wieckowski, M. R., Giorgi, C., Lebiedzinska, M., Duszynski, J. and Pinton, P. (2009). Isolation of mitochondria-associated membranes and mitochondria from animal tissues and cells. *Nat. Protoc.* **4**, 1582-1590.

Wu, Z., Puigserver, P., Andersson, U., Zhang, C., Adelmant, G., Mootha, V., Troy, A., Cinti, S., Lowell, B., Scarpulla, R. C. et al. (1999). Mechanisms controlling mitochondrial biogenesis and respiration through the thermogenic coactivator PGC-1. *Cell* **98**, 115-124.

Xiao, Y., Karnati, S., Qian, G., Nenicu, A., Fan, W., Tchatalbachev, S., Höland, A., Hossain, H., Guillou, F., Lüers, G. H. et al. (2012). Cre-mediated stress affects sirtuin expression levels, peroxisome biogenesis and metabolism, antioxidant and proinflammatory signaling pathways. *PLoS ONE* **7**, e41097.

Yang, X., Song, Y. and Kong, Q. (2013). Diagnosis and surgical treatment of progressive pseudorheumatoid dysplasia in an adult with severe spinal disorders and polyarthropathy. *Joint Bone Spine* **80**, 650-652.

Zampese, E., Fasolato, C., Kipanyula, M. J., Bortolozzi, M., Pozzan, T. and Pizzo, P. (2011). Presenilin 2 modulates endoplasmic reticulum (ER)-mitochondria interactions and Ca2+ cross-talk. *Proc. Natl. Acad. Sci. USA* **108**, 2777-2782.

Zhou, C., Huang, Y., Shao, Y., May, J., Prou, D., Perier, C., Dauer, W., Schon, E. A. and Przedborski, S. (2008). The kinase domain of mitochondrial PINK1 faces the cytoplasm. *Proc. Natl. Acad. Sci. USA* **105**, 12022-12027.

Zhou, R., Yazdi, A. S., Menu, P. and Tschopp, J. (2011). A role for mitochondria in NLRP3 inflammasome activation. *Nature* **469**, 221-225.

Zhou, H., Zheng, C., Su, J., Chen, B., Fu, Y., Xie, Y., Tang, Q., Chou, S.-H. and He, J. (2016). Characterization of a natural triple-tandem c-di-GMP riboswitch and application of the riboswitch-based dual-fluorescence reporter. *Sci. Rep.* **6**, 20871.